Canonical spin glass and cluster glass behavior in the polymorphs of $LiFeSnO_4$

Souvik Banerjee, Debendra Prasad Panda, Premakumar Yanda, and A. Sundaresan*
School of Advanced Materials, and Chemistry and Physics of Materials Unit, Jawaharlal Nehru Centre for Advanced Scientific Research, Jakkur, Bengaluru – 560064, India

(Received 20 September 2022; revised 14 December 2022; accepted 2 March 2023; published 16 March 2023)

We report a comprehensive and comparative study of structural, static, dynamic, and nonequilibrium magnetic properties on the polymorphs of $LiFeSnO_4$. It exhibits two polymorphs: (i) orthorhombic phase (HT) stabilized at high temperature and (ii) hexagonal phase (LT) obtained at lower synthetic temperature. The HT phase crystallizes in the orthorhombic structure (space group: *Pmcn*) and exhibits a site disordered, nonfrustrated zig-zag network of Fe^{3+} and Sn^{4+} ions. On the other hand, the LT phase shows a disordered frustrated kagome network of Li^{1+}, Fe^{3+}, and Sn^{4+} ions crystallizing in the hexagonal structure (space group: $P6_3mc$). The low-temperature thermo-magnetic irreversibility and the absence of heat capacity anomaly in both polymorphs indicate the absence of long-range magnetic ordering and a possible glassy state. Zero-field-cooled and field-cooled magnetic memory effect and spin relaxation measurements stipulate the spin glass nature of the polymorphs. Further, spin glass behavior is confirmed by the AC susceptibility measurements. Interestingly, these polymorphs reveal different classes of spin glass states. The site disordered HT phase exhibits a single spin-flip time $\tau_0 \sim 3 \times 10^{-13}$ sec, indicating a canonical spin glass state. In contrast, LT phase, which is disordered and geometrically frustrated, shows the spin-flip time of $\tau_0 \sim 9 \times 10^{-10}$ sec, suggesting a cluster spin glass state. In addition, the exchange bias effect was observed due to magnetic inhomogeneity in both polymorphs.

DOI: 10.1103/PhysRevMaterials.7.034405

I. INTRODUCTION

Spin glasses (SG) have been an exciting class of magnets for decades and are still a topic of fundamental interest [1,2]. Quantum mechanically, it can be depicted as a magnetic material having a large degenerate ground state with spins frozen in random directions upon cooling the system from its paramagnetic region. It is very well known that magnetic frustration in the system can lead to a spin glass state. However, in some compounds, coexistences of long-range magnetic ordering and spin glass state were observed [3–5]. The magnetic frustration is caused due to competing ferromagnetic and antiferromagnetic interactions mediated by geometrical frustration or by random quenched disorder [1,2,6]. Different types of lattices like triangular, square, kagome, hyperkagome, and pyrochlore structures containing Ising spin at each site are well-known hosts for creating geometry-mediated magnetic frustration [7–11]. In quenched disorder systems, different atoms are randomly distributed at a particular crystallographic site [12], and if the disorder involves the interchange of metal ions within themselves, it is referred as site disorder [13]. Depending on the spin freezing, spin glass can be of two types: one is cluster glass where atomic spins form spin clusters in a ferromagnetic or antiferromagnetic fashion and these spin clusters are frozen upon cooling from the paramagnetic region, and the other one is canonical spin glass where atomic spins are frozen without forming any spin clusters [14]. No one-to-one correspondence exists between canonical spin glass and cluster glass with geometrical frustration and magnetic site disorder. Cluster spin glass can originate from a site disorder like $Cr_{0.5}Fe_{0.5}Ga$ [15] or a geometrically frustrated systems like layered Mn-based triangular lattice compound $Li_2Mn_3O_7$ [7]. Similarly, canonical spin glass can originate either from site disordered systems, such as disordered half-Heusler compound IrMnGa [14], or geometrically frustrated lattices like $YbZnGaO_4$ [8].

Lithium stannoferrites are known for their rich structural chemistry and polymorphism [16,17]. It has been extensively studied for Li-ion batteries in the last decades [18,19]. It has two polymorphs; the high-temperature (HT) phase crystallizes in orthorhombic structure, and the low-temperature (LT) phase crystallizes in a hexagonal structure. In the HT phase, all the Fe and Sn atoms occupy the same crystallographic position, forming a site disordered magnetic systems in a nonfrustrated isolated zig-zag lattice. On the other hand, the LT phase shows a frustrated quasi-2D kagome lattice with the magnetic disorder at crystallographic site 6*c* [16,20]. This interesting and distinguishable crystal chemistry motivated us to investigate the magnetic properties in polymorphs of $LiFeSnO_4$. In this article, we report various equilibrium, nonequilibrium, and dynamical magnetic properties on the polymorphs of $LiFeSnO_4$. Equilibrium properties like DC magnetization, heat capacity, and nonequilibrium magnetic properties like magnetic relaxation, zero-field-cooled (ZFC), and field-cooled (FC) memory effect suggest spin glass state in both polymorphs. Our detailed investigation of dynamical magnetic properties of the polymorphs establishes a canonical spin glass state with a spin flipping time of the order of atomic spin-flip ($\sim 10^{-13}$ sec) for a complete site disordered HT phase. In contrast, the LT phase with site disorder hosted by a frustrated kagome net shows a cluster spin glass ground

*sundaresan@jncasr.ac.in

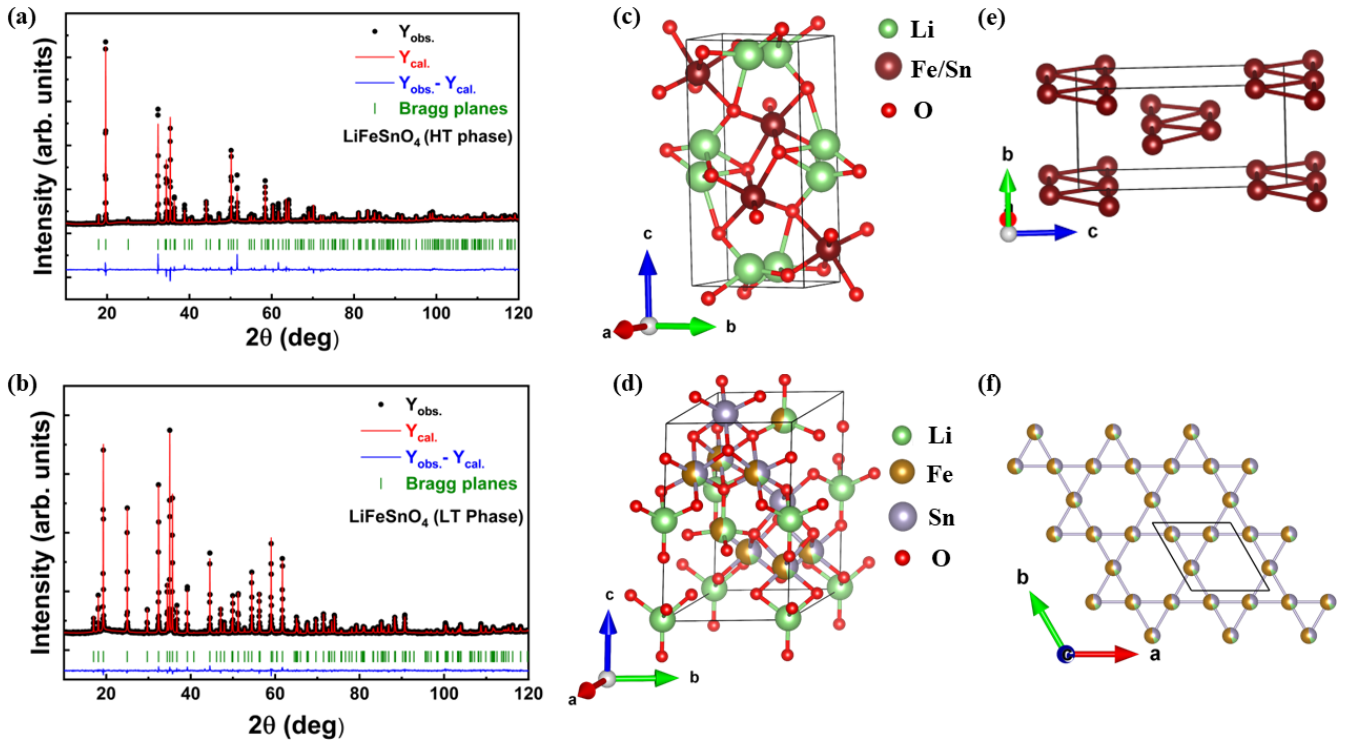

FIG. 1. Rietveld refinement of XRD data for (a) HT phase, and (b) the LT phase. The crystal structures for (c) HT and (d) the LT phases. (e) The zig-zag Fe/Sn disordered network of the HT phase. (f) Distorted kagome lattice of the LT phase for Li/Fe/Sn disorder.

state with much slower (∼3000 times) spin-flip dynamics with respect to atomic spin flip.

II. EXPERIMENTAL

The polymorphs of $LiFeSnO_4$ were synthesized by the conventional solid-state method [16]. First, Li_2CO_3, Fe_2O_3, and SnO_2 in a stoichiometric ratio were mixed thoroughly and calcinated at 600 °C and 900 °C for 12 h each. The resulting product was ground, pelletized, and sintered at 1200 °C for 12 h, followed by quenching of the sample in liquid N_2 to obtain the pure orthorhombic (HT) phase. To synthesize the hexagonal (LT) phase, HT phase was sintered at 800 °C for 12 h, followed by cooling to room temperature at the rate of 5 K/min. To investigate the phase purity and crystal structure of the compounds, we have performed powder x-ray diffraction (XRD) measurement at room temperature using PANalytical Empyrean diffractometer with monochromatic Cu Kα_1 radiation ($\lambda = 1.5406$ Å). Rietveld refinement of the powder XRD data was performed using FULLPROF software [21]. DC magnetic measurements were carried out using Magnetic Property Measurement System (MPMS-superconducting quantum interference device, Quantum Design, USA). The heat capacity and AC magnetic susceptibility measurements were performed in Physical Property Measurement System (PPMS, Quantum Design, USA).

III. RESULTS AND DISCUSSIONS

A. Crystal structure

Rietveld refinement were performed on the room temperature powder XRD data of HT and LT polymorphs and the refined data are shown in Figs. 1(a) and 1(b), respectively. The HT phase crystallizes in orthorhombic *Pmcn* structure whereas the LT phase exhibits $P6_3mc$ crystal structure. The refined structural parameters are given in Tables I and II,

TABLE I. Structural parameters of the HT phase obtained from Rietveld refinement of room temperature powder XRD data. Space group: *Pmcn*; $a = 3.0666(1)$ Å, $b = 5.0721(1)$ Å, $c = 9.8766(1)$ Å, $V = 153.622(2)$ Å^3. $\chi^2 = 5.97$, $R_p = 2.84\%$, $R_{wp} = 4.32\%$.

Atom	Site	x	y	z	Occupancy	B_{iso}(Å^2)
Li1	4*c*	1/4	0.9350[a]	0.4326(436)	0.156(78)	1.0
Li2	4*c*	1/4	0.9720[a]	0.5635(188)	0.344(78)	1.0
Fe	4*c*	1/4	0.9839(11)	0.1414(4)	0.5	0.106(76)
Sn	4*c*	1/4	0.9839(11)	0.1414(4)	0.5	0.106(76)
O1	4*c*	1/4	0.6710(60)	0.2913(24)	1.0	1.0
O2	4*c*	1/4	0.2237(40)	−0.0430(25)	1.0	1.0

[a]We have fixed the y coordinate of Li1 and Li2 to achieve a stable Rietveld refinement.

TABLE II. Structural parameters of the LT phase obtained from Rietveld refinement of room temperature powder XRD data. Space group: $P6_3mc$; $a = b = 6.0057(1)$ Å, $c = 9.7743(2)$ Å, $V = 305.310(4)$ Å^3. $\chi^2 = 2.00$, $R_p = 1.83\%$, $R_{wp} = 2.35\%$.

Atom	Site	x	y	z	Occupancy	B_{iso}(Å^2)
Li1	2b	1/3	2/3	−0.0926(16)	0.094(2)	1.243(372)
Fe1	2b	1/3	2/3	−0.0926(16)	0.073(2)	1.243(372)
Li3	2a	0	0	0.5100[a]	0.167	1.0
Sn1	2b	1/3	2/3	0.4970[a]	0.167	0.353(63)
Sn2	6c	0.1680(3)	−0.1680(3)	0.2189(4)	0.167	0.604(66)
Li2	6c	0.1680(3)	−0.1680(3)	0.2189(4)	0.066(5)	0.604(66)
Fe2	6c	0.1680(3)	−0.1680(3)	0.2189(4)	0.267(5)	0.604(66)
O1	2a	0	0	0.3223(25)	0.167	1.0
O2	2b	1/3	2/3	0.1131(25)	0.167	1.0
O3	6c	0.4902(9)	−0.4902(9)	0.3577(21)	0.5	1.0
O4	6c	0.1612(22)	−0.1612(22)	0.6082(23)	0.5	1.0

[a]We have fixed the z coordinate of Li3 and Sn1 to obtain a stable Rietveld refinement.

respectively. In the HT phase, Fe and Sn ions are completely disordered (Fe ∼ 50%, and Sn ∼ 50%) at a crystallographic site 4c in a distorted oxygen octahedra, as shown in Fig. 1(c). There are two different crystallographic 4c sites for Li ion in distorted tetrahedral oxygen coordination and both Li sites are partially vacant. This disordered Fe/Sn site exhibits an isolated Zig-Zag network represented in Fig. 1(e). In the LT phase, Li, Fe, and Sn ions are disordered (Li ∼ 13.3%, Fe ∼ 53.3%, and Sn ∼ 33.3%) at crystallographic site 6c with a distorted square pyramidal of oxygen coordination, as shown in Fig. 1(d). This disordered 6c site forms a frustrated kagome network of length 3.027 Å [Fig. 1(f)]. There is another disorder between Li and Fe (Li ∼ 63% and Fe ∼ 37%) in crystallographic site 2b in distorted oxygen tetrahedral coordination. Our results are consistent with earlier reports [16,17,20,22,23]. The other magnetic disorder position at crystallographic site 2b, occupied by Li (∼63.1%) and Fe (∼36.9%) affects the magnetic interaction in the disordered kagome plane.

B. DC magnetization and heat capacity

We have measured the temperature-dependent magnetization (M) under different magnetic fields (H) for both HT and LT polymorphs in ZFC and FC protocols. There is a distinguishable bifurcation between ZFC and FC magnetization measured under a 100 Oe magnetic field at the temperature known as irreversible temperature $T_{irr} \sim 20.2$ K and 15.7 K for HT and the LT phases, respectively, suggesting the existence of thermo-magnetic irreversibility in the systems, as shown in Figs. 2(a) and 2(b). This irreversibility generally results from superparamagnetic or spin glass behavior in the system [23]. To investigate the behavior of the thermomagnetic irreversibility, ZFC and FC moments were measured under different magnetic fields. Figures 2(c) and 2(d) show the bifurcation between ZFC and FC moment persists until 1000 Oe, where the bifurcation temperature T_{irr} decreases with increasing magnetic field H; indicating spin freezing or possible glassy state below the bifurcation temperature. To understand the role of magnetic field on thermomagnetic irreversibility, the analysis of H-T_{irr} phase diagram is important, where two irreversible line can arise depending on the spin irreversibility in a frozen state: Gabby-Toulouse (GT) and de Almeida-Thouless (AT) lines [3,24]. In the weak magnetic field region, the AT line follows with $H^{2/3}$ dependency of T_{irr} due to strong irreversibility or strong spin anisotropy in spin-frozen state. Whereas, in the strong magnetic field region, due to weak irreversibility, the GT line follows H^2 dependency of T_{irr}. The magnetic field (H) variation of irreversible temperature (T_{irr}) has been fitted with the following:

$$T_{irr}(H) = T_{irr}(0)(1 - CH^n). \quad (1)$$

Here $T_{irr}(0)$ represents spin glass temperature, n represents determining factor for the AT or GT line in the H-T_{irr} diagram known as crossover exponent, and C as a constant. From the fitting of H-T_{irr} with the Eq. (1) shown in Figs. 2(e) and 2(f), we obtained the value of $n = 0.64 \pm 0.17$ and 0.79 ± 0.09 for the LT and HT polymorphs, respectively, which is close to the theoretically predicted value of 2/3 for mean-field Ising spin glass with strong irreversibility.

Isothermal magnetization was measured for both HT and the LT phases at different temperatures. The linear dependence of isothermal magnetization (M) on magnetic field (H) at 100 K gives the essence of paramagnetic behavior, as shown in Figs. 3(a) and 3(b). Below 30 K, the isothermal magnetization curves became S-shaped indicating the possibility of glassy spin state in the samples. The small hysteresis loop at the lowest temperature of 2 K for the HT and LT polymorphs are consistent with spin glass nature in the samples. So, the lower value of magnetization at 70 kOe (0.41 $\frac{\mu_B}{f.u}$ for HT and 0.68 $\frac{\mu_B}{f.u}$ for LT), the hysteresis loops, and S-shaped isothermal magnetization at 2 K indicate the possibility of spin glass state in both the polymorphs. To further examine the presence of any long-range magnetic ordering, we have carried out heat capacity measurements for both phases and the results are depicted in Figs. 3(c) and 3(d). The absence of any anomaly confirms the T_{irr} is not associated with any long-range magnetic order. The presence of hump in the plot of C_p/T vs T plot shown in the inset of Figs. 3(c) and 3(d), further supports the absence of long-range magnetic ordering and presence of frozen spin state. The low temperature heat capacity data from 2 to 5 K was fitted with the empirical formula $C_P = \gamma T + \beta T^3 + \delta T^{3/2}$, shown in the inset of

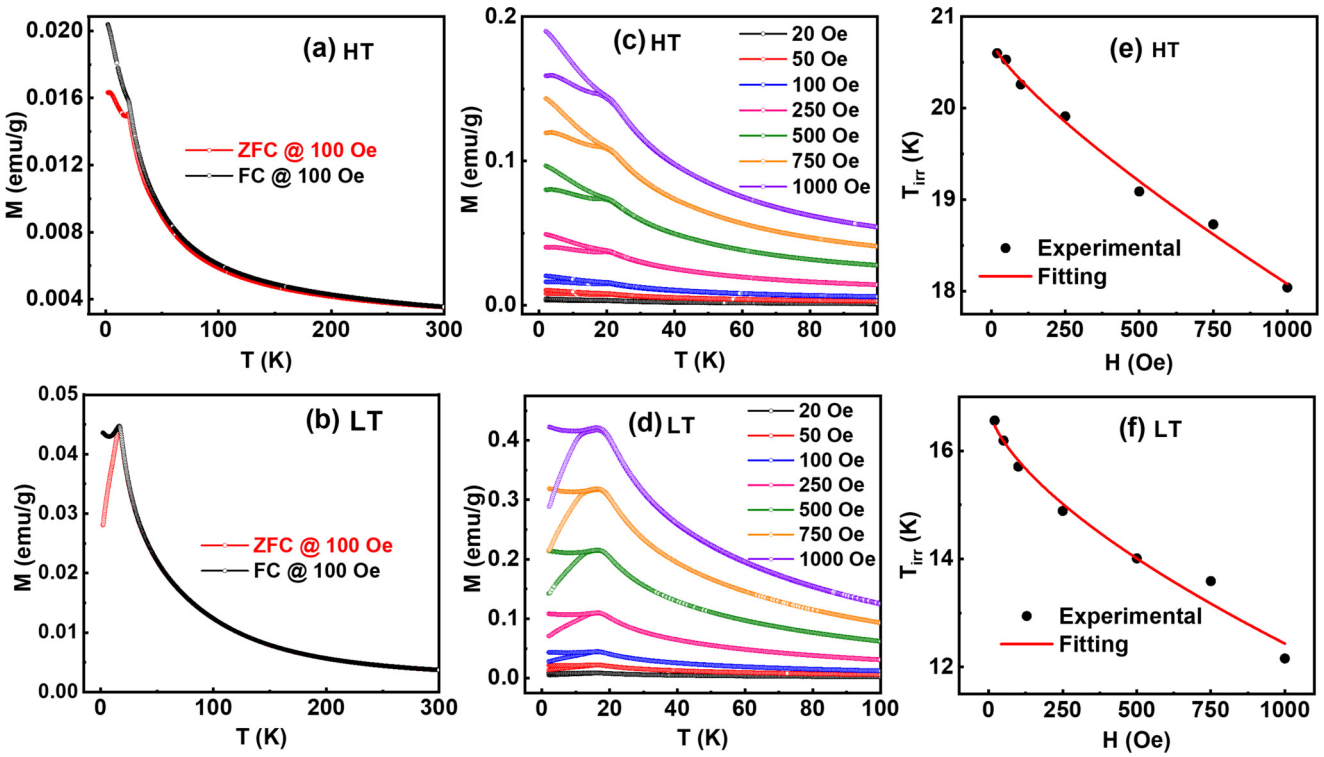

FIG. 2. Temperature dependent ZFC and FC magnetization at 100 Oe for (a) HT and (b) the LT phase. ZFC and FC magnetization under different magnetic fields for (c) HT and (d) the LT phase. The de Almeida-Thouless (AT) line fitting for (e) HT and (f) the LT polymorphs.

Figs. 3(c) and 3(d). Here γ is the electronic (or fermionic to be specific) contribution, β is the phonon contribution to specific heat and δ is the extra term due to spin glass contribution. We obtained Sommerfeld coefficient $\gamma \sim 67$ and $70\,\mathrm{mJ\,mol^{-1}\,K^{-2}}$ for the HT and LT phases, respectively, which is quite large for a conventional insulators with few

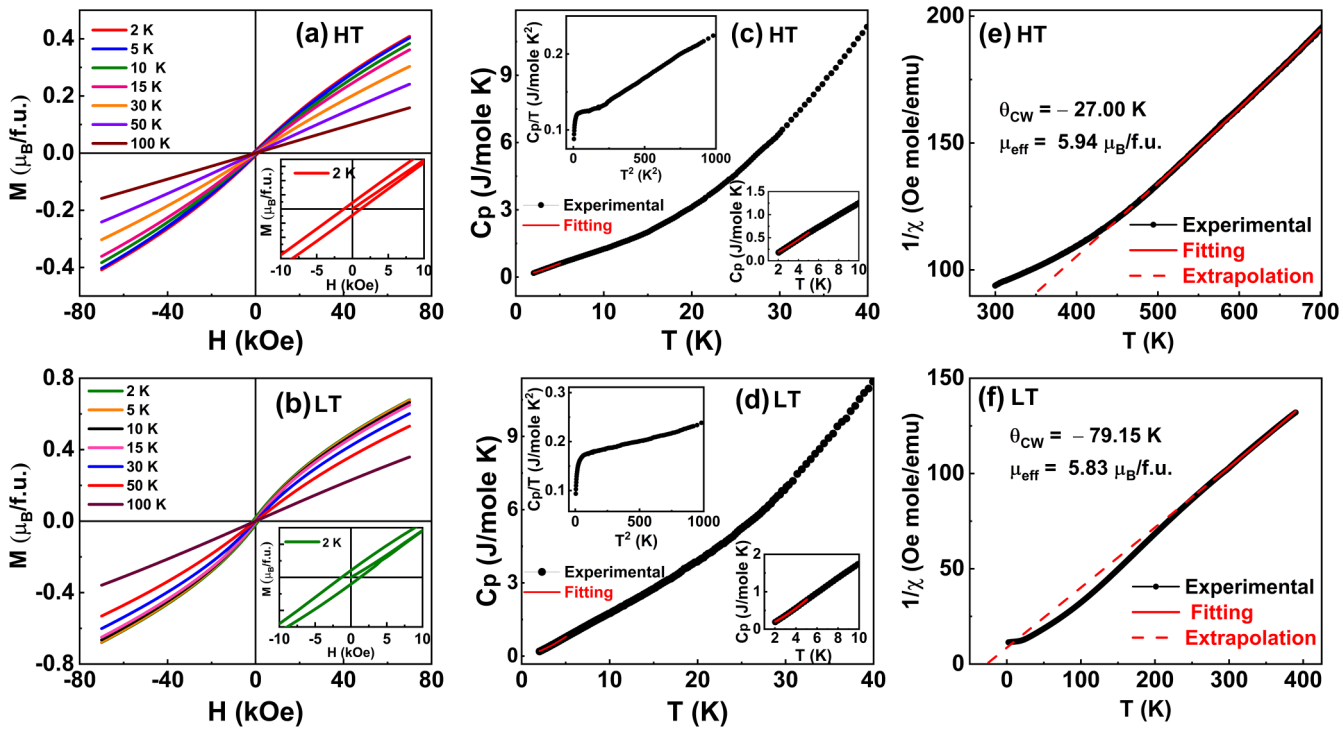

FIG. 3. Isothermal magnetization at different temperatures for (a) HT and (b) the LT polymorphs. (c) and (d) Temperature-dependent specific heat capacity with fittings shown in insets for both phases, respectively. Curie- Weiss fitting for (e) HT and (f) the LT polymorphs.

rare reports [25,26]. This may be because of the contribution coming from electronlike (or fermionic) excitons, which do not conduct electricity but heat [25–32]. We obtained phonon contribution term $\beta \sim 0.09$ and $0.74\,\mathrm{mJ\,mol^{-1}\,K^{-4}}$ for HT and the LT phases, respectively, resulting in Debye temperature $\theta_D \sim 532$ and 264 K [$\theta_D = (\frac{12\pi^4 RN}{\beta})^{1/3}$]. Furthermore, δ turns out to be 20 and $29\,\mathrm{mJ\,mol^{-1}\,K^{-5/2}}$ for the HT and LT phases, respectively. Furthermore, to know the type and scale of magnetic interaction and the effective paramagnetic moment, we performed fitting of inverse susceptibility data with modified Curie-Weiss law [$\chi = \chi_0 + C/(T - \Theta_{CW})$], shown in Figs. 3(e) and 3(f), in the temperature range 500−700 K for the HT phase (due to presence of quasi-2D isolated zig-zag lattice) and 280−390 K in the LT phase. Here χ_0 is the diamagnetic contribution. The Curie-Weiss temperature Θ_{CW} was obtained to be ∼−27.0 K and −79.2 K for the HT and LT phases, respectively, indicating predominantly antiferromagnetic interaction. The effective paramagnetic moment $\mu_{\mathrm{eff}} \sim 5.98$ and 5.83 $\frac{\mu_B}{f.u}$ for HT and LT phases, respectively, are close to theoretically μ_{eff} (5.92 $\frac{\mu_B}{f.u}$ of Fe^{3+}). The empirical frustration index, f ($\frac{\Theta_{CW}}{T_{irr}}$) turns out to be 1.3 and 5.1 for the HT and the LT phases respectively. This qualitative analysis of frustration index indicates that the LT phase is much more frustrated than the HT phase.

C. Nonequilibrium dynamics

DC magnetization and heat capacity studies indicated a spin glass state with short-range magnetic interactions in both phases. To get a better insight into the short-range magnetic fluctuation and frozen spin state, various nonequilibrium magnetic properties such as magnetic relaxation, ZFC, and FC memory effects were carried out. To investigate magnetic relaxation, the magnetic moment was measured with time after cooling down the sample from a paramagnetic region to a temperature below T_{irr} under a magnetic field of 100 Oe, in a demagnetizing protocol [1]. The magnetic relaxation has been fitted with Eq. (2), as shown in Figs. 4(a) and 4(b),

$$\mathrm{M(t)} = \mathrm{M_0} + \mathrm{M_g e^{-(t/\tau)^{\beta}}}. \tag{2}$$

Here, M(t), $\mathrm{M_0}$, and $\mathrm{M_g}$ account for instantaneous magnetization, a bulk ferromagnetic component that sustains upon removal of the external magnetic field, and the glassy component of the magnetic moment that diminishes over time. The parameters τ and β stand for relaxation time and relaxation rate, respectively. In the absence of a metastable state in the system, $\beta = 0$, reveals no magnetic relaxation. But, when $\beta = 1$, the system possesses a uniform energy barrier between the excited nonrelaxed and relaxed ground states [15]. So, for a spin glass compound that lacks a uniform energy barrier and evolves through different metastable states, where β lies between 0 and 1. The obtained fitting parameters are shown in Table III. We have obtained $0 < \beta < 1$ for all the temperatures below the spin glass temperature for both the phases, which reveals that the systems are evolving through a number of intermediate metastable states over anisotropic energy barriers [33,34].

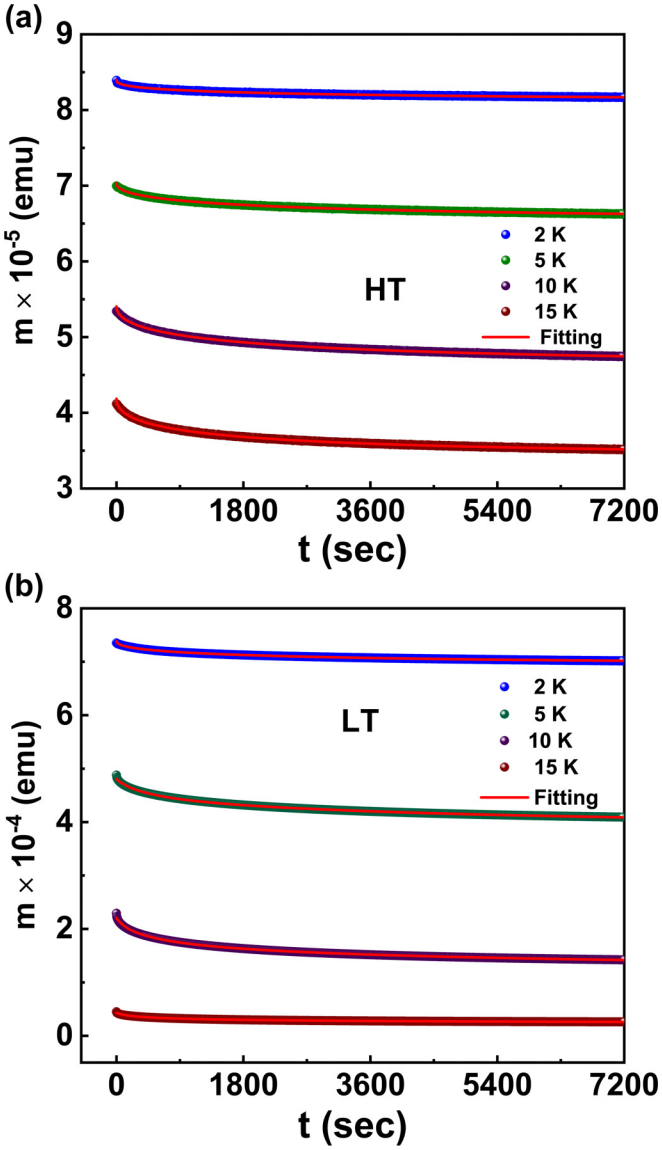

FIG. 4. The magnetic relaxation at different temperatures for (a) HT and (b) the LT phases.

The magnetic memory effect is another characteristic feature of spin glass compound, resulting from short-range magnetic ordering and magnetic relaxation. Memory effect in both phases is probed using zero-field-cooling (ZFC memory effect) and field-cooling (FC memory effect) protocols [23]. In the ZFC protocol, we first cool down the samples from

TABLE III. Parameters obtained from fitting of magnetic relaxation.

	HT phase		LT phase	
Temperature (K)	τ (sec)	β	τ (sec)	β
2	3067	0.4283	2843	0.4707
5	2020	0.4818	2192	0.4993
10	2054	0.4933	1435	0.4771
15	1488	0.4861	1012	0.4578

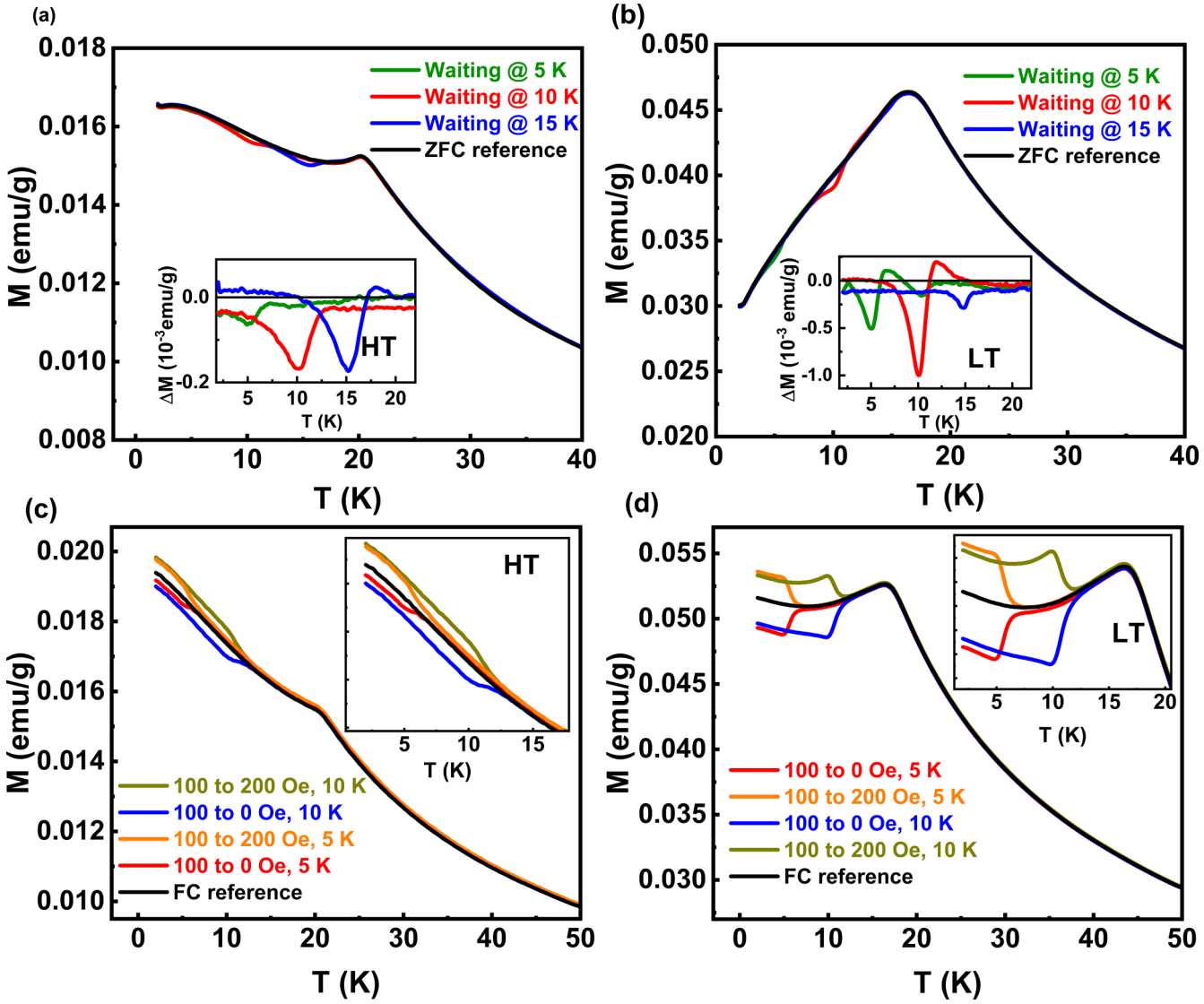

FIG. 5. Zero-field-cooled (ZFC) memory effect at different temperatures for (a) HT and (b) the LT phase. (c) and (d) Field-cooled memory effect (FC memory) interrupted at temperatures 10 and 5 K by magnetic field 100 Oe with a time delay of 3600 sec.

paramagnetic region to a temperature below T_{irr} without applying magnetic field, and wait 1 h at that temperature before cooling down to 2 K. We measured magnetic moment while warming under a 100 Oe magnetic field. The procedure was repeated varying the waiting temperatures ($T = 5$, 10, and 15 K). For measuring ZFC reference, we followed the same protocol without any waiting time. All these plots for different phases are shown in Figs. 5(a) and 5(b), respectively. There is a dip in magnetic moments with respect to ZFC reference at those waiting temperatures. At the waiting temperatures, the magnetic cluster relaxes to attain a local minimum energy owing to the magnetic relaxation of the system. The average energies in these magnetic clusters are insufficient to overcome the energy barrier between the local minima and the global minima. At local minima, the magnetic entities are relaxed with fewer moments and are confined. While measuring the magnetic moment with increasing temperature, the clusters achieve the local minima and show a relaxed moment value, less than that of the ZFC reference [1,35,36].

According to the spin glass model of short-range interaction [37], the FC state is paramagnetic. But, mean field theory suggests field cooling brings in an equilibrium state [2] where no memory effect is expected. Though there are some reports on the memory effect in magnetic nanoparticles [38–40] and canonical spin glass system [41], the effect of perturbation of magnetic field was not understood well in different classes of spin glass. So we have performed FC memory on both the polymorphs by the protocol followed by Roy *et al.* [41]. The sample was cooled from paramagnetic region to a certain temperature below T_{irr} under 100 Oe magnetic field. The magnetic field was increased to 200 Oe followed by a wait time of one hour. After waiting, the magnetic field was reduced to 100 Oe again and the sample was cooled to 2 K. The magnetic moment was measured in warming cycle. In another set, we followed a similar protocol except the magnetic field was changed from 100 to 0 Oe. FC reference was measured in conventional FC measurement protocol in 100 Oe while warming from 2 K and depicted in Figs. 5(c) and 5(d) for both

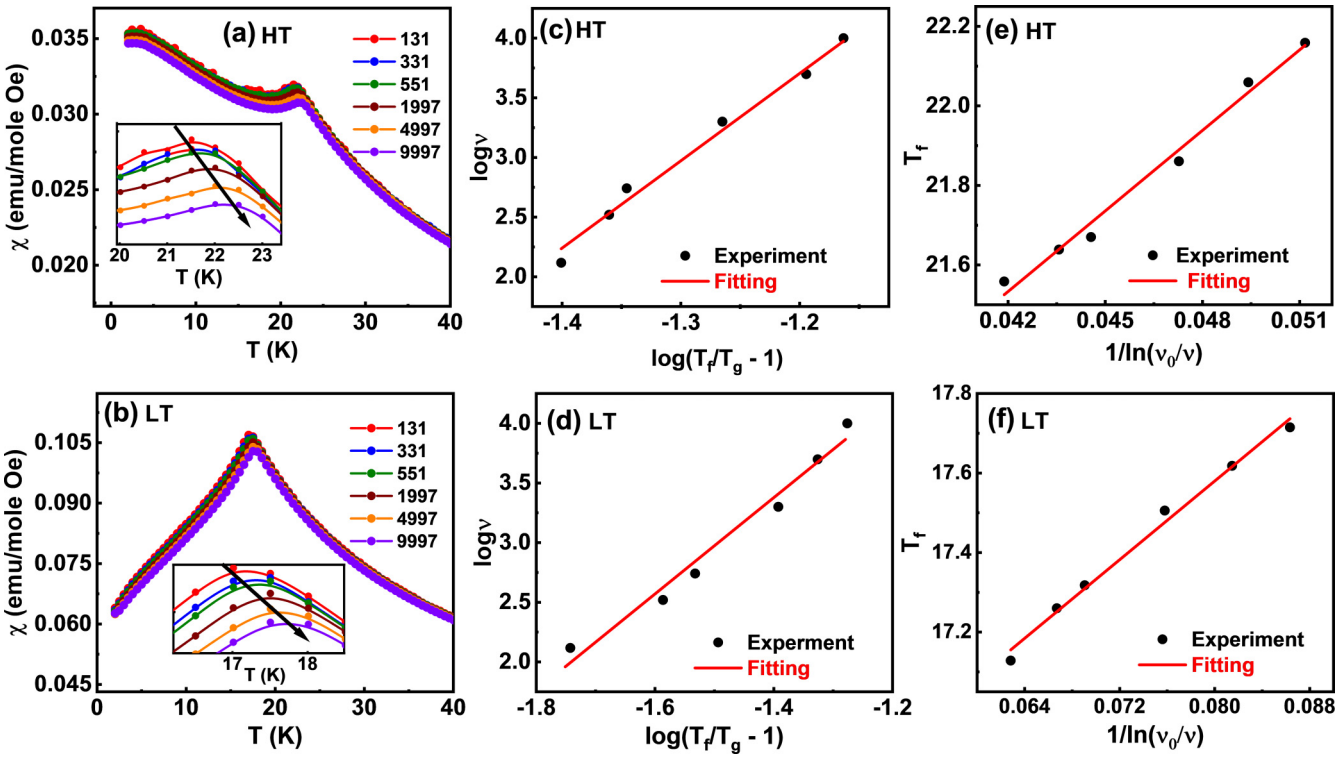

FIG. 6. (a) and (b) Frequency-dependent ac magnetic susceptibility and relative shift of spin freezing temperature T_f. (c) and (d) Power law fitting of the shift of T_f with υ. (e) and (f) VF fitting for HT and the LT polymorphs, respectively.

polymorphs. The deviation of magnetic moment at 10 and 5 K with respect to reference indicates the FC memory effect. The bifurcation of magnetization data for different magnetic field (0 or 200 Oe) shows that the FC state can also remember any perturbation in magnetic field to its Hamiltonian. So, the FC state energy landscape is also rugged in presence and absence of external magnetic field [41], which is contradictory to the short-range interaction model [37] and mean field model [42]. This suggests the FC state of a spin glass compound is paramagnetic [37] and lies in equilibrium [42].

D. AC susceptibility

Frequency-dependent magnetic measurements were carried out to understand the spin freezing dynamics of spin glass state of the polymorphs under 10 Oe ac magnetic field in ZFC protocols. Figures 6(a) and 6(b) show that the spin freezing temperature T_f (the position of maxima) is shifting towards higher temperature with an increase of the frequency of the ac magnetic field with a dispersion of ac magnetic susceptibility below T_f confirming the spin glass nature of both the systems. The frequency sensitivity of spin freezing was determined by the Mydosh parameter, which measures relative peak shift with change of frequency. The expression for the Mydosh parameter s is given by

$$s = \frac{\Delta T_f}{T_f \Delta \log_{10}(\upsilon)}, \tag{3}$$

where $\Delta T_f = T_f(\upsilon_1) - T_f(\upsilon_2)$, $\Delta log_{10}(\upsilon) = \log_{10}(\upsilon_1) - \log_{10}(\upsilon_2)$, $T_f = T_f|_{\text{minimum}}$.

For strongly interacting entities, a large amount of frequency difference is needed to observe a detectable amount of peak shift. As a result, a system with stronger magnetic interacting entities is less frequency sensitive than that of weakly interacting clusters. For a spin glass system, the value of s lies between 0.001 and 0.081. The Mydosh parameter was obtained to be 0.015 and 0.018, which rules out the possibility of a superparamagnetic state ($s > 0.2$), confirming the spin glass state of the polymorphs. To get an insight about spin glass nature of the polymorphs, the frequency dependency of spin freezing temperature T_f has been studied through different scaling laws. According to the power law, the T_f can be expressed as [1,2],

$$\tau = \tau_0 (T_f/T_g - 1)^{-z\upsilon'}, \tag{4}$$

where τ represents slowed down relaxation time due to the application of external frequency υ ($\frac{1}{\tau}$). τ_0 accounts for intrinsic characteristic single spin-flip time, T_g is spin glass temperature ($T_{irr}(0)$), T_f = spin freezing temperature. Thus Eq. (4) can alternatively be written as

$$T_f = T_g\{1 + (\upsilon\tau_0)^{\frac{1}{z\upsilon'}}\}. \tag{4a}$$

Equation (4a) stipulates that the spin freezing temperature increases with an increasing frequency indicating slowing down the spin flip. This is being referred as critical slowing down [43]. Here, z is the dynamical critical constant and υ' is critical exponent representing the correlation length as $\xi \sim (T_f/T_g - 1)^{-\upsilon'}$ and the slowed down relaxation time τ can be corelated as $\tau \sim \xi^z$. This power law can be fitted with the

TABLE IV. Parameters obtained from the power law and VF fittings of ac susceptibility data.

	Power law fitting			VF fitting			
Phase	zv'	τ_0 (sec)	τ_{0LT}/τ_{0HT}	E_a/k_B (K)	T_0 (K)	$t = T_0k_B/E_a$	t_{LT}/t_{HT}
HT	7.3 ± 0.5	3×10^{-13}	3000	67.51	18.70	0.27	2.3
LT	4.0 ± 0.3	9×10^{-10}		24.71	15.60	0.63	

following linearized equation:

$$\log_{10}\upsilon = \log_{10}\upsilon_0 + zv' \log_{10}(T_f/T_g - 1) \quad (4b)$$

The intrinsic characteristic single spin-flipping time τ_0 is given by $\tau_0 = 10^{-\log_{10}\upsilon_0}$ We have fitted this linearized power law equation (4b) for both HT and the LT polymorphs shown in Figs. 6(c) and 6(d). The fitted parameters are given in Table IV. The τ_0 values for a typical canonical spin glass lie in between 10^{-12} to 10^{-14} sec [35], which is comparable to the single spin-flip time of atomic magnetic moments (10^{-13} sec). In contrast, for a cluster glass, τ_0 lies between 10^{-7} to 10^{-10} sec [44]. The intrinsic characteristic spin-flip time of the HT phase is $\sim 3 \times 10^{-13}$ sec, which lies in the canonical spin glass regime. Whereas for the LT phase, τ_0 is $\sim 9 \times 10^{-10}$ sec. The slowing down of intrinsic relaxation by 3×10^3 order of magnitude clearly indicates the existence of interacting larger spin clusters in the LT phase [2,43,45]. The obtained zv' falls under spin glass regime of value 3 to 10.

Besides the power law, Vogel-Fulcher (VF) law can give an insight about the interaction strength between the magnetic entities [35] given by Eq. (5)

$$\tau = \tau_0 \exp\{E_a/k_B(T_f - T_0)\}. \quad (5)$$

The VF law deals with systems having sufficiently large τ. However, the difference looks visible when the variation of τ approaches 10^{-11} order of magnitude. This explains the usefulness phenomenological VF law to explain the glassy behavior of spin glass [46]. The equation can be further written as

$$T_f = \frac{E_a}{k_B \ln\left(\frac{\upsilon_0}{\upsilon}\right)} + T_0, \quad (5a)$$

where E_a is the average activation energy of spin flipping, and T_0 is the VF temperature which is a measure of intercluster coupling strength. We have fitted the experimental data points with linearized VF equation (5a) (values of υ_0 taken from power law fitting) shown in Figs. 6(e) and 6(f), and the fitting parameters are given in Table IV. Here, $T_0 \ll E_a/k_B$ indicates a weaker coupling between interclusters and $T_0 \gg E_a/k_B$ for a stronger one. The ratio t, T_0k_B/E_a can be used as a parameter to understand the interaction. A large value of t indicates strong intercluster coupling [47]. As seen from Table IV, $t_{LT} \sim 2.3t_{HT}$. Moreover, the Tholence criterion ($\delta T = (T_f - T_0)/T_0$) [48] turns out to be $\sim$0.13 and 0.14 for HT and the LT polymorphs, respectively, which comes under the spin glass regime [49].

The systems with stronger magnetic interaction between different magnetic clusters should relax more slowly than those with weaker magnetic interaction. The entities with comparatively stronger magnetic interaction ($t = 0.63$) in the LT phase relax slowly with higher intrinsic spin-flip time ($\tau_0 \sim 10^{-10}$ sec) than that of the entities with comparatively weaker magnetic interaction ($t = 0.27$), which relaxes faster with shorter spin-flip time ($\tau_0 \sim 10^{-13}$ sec). So, the LT phase consists of magnetic entities interacting more strongly than the entities in the HT phase, representing the LT phase as cluster glass and the HT phase as canonical spin glass.

Magnetic frustration is the thing which is dictating the system to be spin glass. This frustration can arise either by site disorder or geometrical frustration or both. In the HT phase the 4*c* site is randomly occupied by Fe^{3+} and Sn^{4+} ion with total 50% occupancy each and this random distribution of magnetic and nonmagnetic ion (with same number of Fe^{3+} and Sn^{4+} as a whole) is the ingredient of magnetic frustration in HT phase. On the other hand, in the LT phase there are two disorder site: 2*b* site with random distribution of Li^{1+} (56.26%) and Fe^{3+} (43.72%) and 6c site with random distribution of Li^{1+} (33.4%), Fe^{3+} (53.4%), and Sn^{4+} (13.2%). Both the site disorder contributes to the magnetic frustration. The 6*c* site forms a Kagome lattice which is also a geometrically frustrated lattice so both the site disorder and geometrical frustration contributes to the magnetic frustration in the LT phase. So, this add on of geometrical frustration in the LT phase is somehow responsible for increasing the frustration to the LT phase than the HT phase and can be extrapolated as the driving force in the canonical to cluster glass crossover in $LiFeSnO_4$.

E. Exchange bias effect

Exchange bias is the experimental outcome of the presence of exchange anisotropy in magnetic materials [50]. Systems with exchange anisotropy attain different magnetic ground states upon cooling the system below the ordering temperature in FC and ZFC protocols [50]. The ZFC hysteresis loop is expected to be symmetric around $H = 0$ Oe in isothermal magnetization. But, in the FC protocol, after cooling down the material in the presence of the external applied magnetic field, the FC hysteresis loop became asymmetric about $H = 0$ Oe. This horizontal and vertical shift of the hysteresis loop is referred to as the exchange bias effect. Materials showing an exchange bias effect are useful for permanent magnet [51], spin valves [52], and spintronic devices [53]. Exchange bias is generally exhibited for the ferromagnetic (FM)-antiferromagnetic (AFM) interface. However, it exists even in systems without clearly defined FM/AFM interfaces. Random arrangements of magnetic ions create certain areas (or domains) with FM/AFM interaction resulting in local exchange anisotropy and exchange bias in spin glasses [50]. The variation of magnetic moment (m) with the magnetic field (H) for different cooling (H_{CF}) is shown in Figs. 7(a) and 7(b) for the HT and LT phases, respectively. The symmetrical hysteresis loop in M vs H data at 2 K shown in Figs. 7(a) and

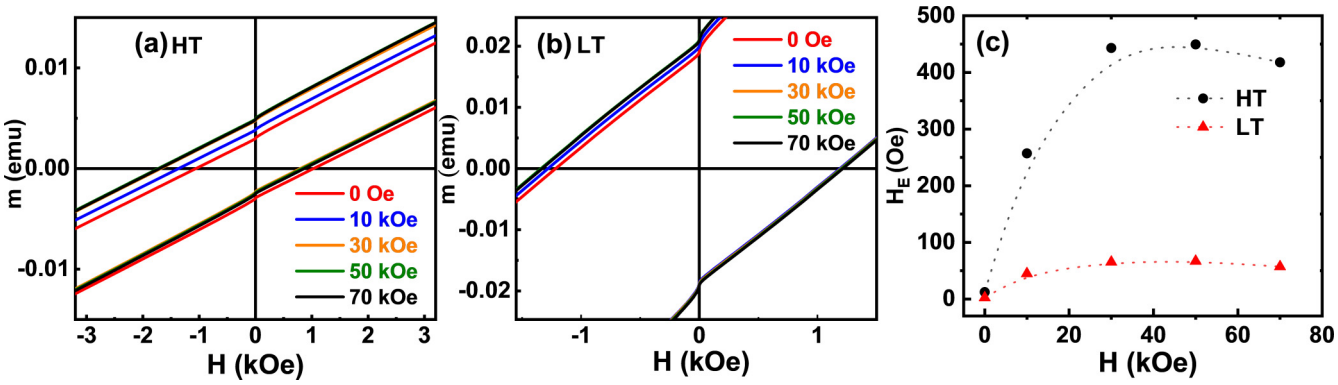

FIG. 7. (a) and (b) Shifting of coercive field under different cooling field (H_{CF}). (c) The variation of exchange bias field for HT and the LT phases.

7(b) for both the samples around $H = 0$ Oe in ZFC protocol rules out the presence of any exchange anisotropy in the ZFC state. The shift of the hysteresis loop in horizontal and vertical direction in FC protocol showing the exchange bias effect in the system under external magnetic field (H_{CF}). The exchange bias field H_E is calculated by the equation $H_E = |\frac{|H_{C1}|-|H_{C2}|}{2}|$. Here the H_{c1} and H_{c2} are the coercive field in positive and negative magnetic cycle. The variation of exchange bias field H_E, with the cooling magnetic field are shown in Fig. 7(c). The maxima in the exchange bias can be explained by local spin arrangement and formation of interacting local FM or AFM clusters. In ZFC isothermal magnetization there is a small symmetrical hysteresis loop at 2 K because of very few ferromagnetic short-range cluster interactions. Upon cooling the system in the presence of H_{CF} there is an alignment of FM clusters in the direction of H_{CF} indicating increase of FM domain and increasing exchange anisotropy in FM/AFM or FM/SG or FM/cluster glass. At higher H_{CF} there might increase of FM domain on the expense of the FM/SG or FM/AFM or FM/cluster glass region so the surface exchange anisotropy decreases resulting in a decrease in exchange bias field [7,54,55].

IV. CONCLUSIONS

We have investigated the structure and the magnetic properties of two polymorphs of $LiFeSnO_4$. The high and low temperature polymorphs crystallize in orthorhombic ($Pmcn$) and hexagonal ($P6_3mc$) structures, respectively. Both polymorphs exhibit a spin glass state at low temperature. The spin-flip time obtained from temperature-dependent ac magnetic susceptibility suggests the HT and the LT polymorphs are canonical spin glass and cluster glass, respectively. This is because the HT polymorph is disordered with no geometrical frustration in the lattice, whereas the LT phase exhibits a disordered frustrated kagome lattice making the LT phase more frustrated than HT. Interestingly, both polymorphs exhibit exchange bias effect below spin freezing temperature. The metastable nature of the FC state was understood by FC memory effect in a cluster glass system for first time. We believe our study will provide an insight into the origin of different nature of spin glass systems and can be studied further as a reference of canonical spin glass to cluster glass crossover by interplay of magnetic site disorder and geometrical frustration by various microscopic probing techniques like inelastic neutron scattering and μSR experiments.

ACKNOWLEDGMENTS

The authors thank Sheik Saqr Laboratory (SSL), International Centre for Materials Science (ICMS), and School of Advanced Materials (SAMat) at Jawaharlal Nehru Centre for Advanced Scientific Research (JNCASR) for various research facilities. S.B. and D.P.P. thank Council of Scientific & Industrial Research (CSIR), India, for fellowship.

[1] K. Binder and A. P. Young, Spin glasses: Experimental facts, theoretical concepts, and open questions, Rev. Mod. Phys. **58**, 801 (1986).

[2] J. A. Mydosh, *Spin Glasses: An Experimental Introduction* (CRC Press, London, 1993).

[3] M. Gabay and G. Toulouse, Coexistence of Spin-Glass and Ferromagnetic Orderings, Phys. Rev. Lett. **47**, 201 (1981).

[4] K. Naveen, M. Reehuis, P. Adler, P. Pattison, A. Hoser, T. K. Mandal, U. Arjun, P. K. Mukharjee, R. Nath, C. Felser, and A. K. Paul, Reentrant magnetism at the borderline between long-range antiferromagnetic order and spin-glass behavior in the B-site disordered perovskite system $Ca_{2-x}Sr_xFeRuO_6$, Phys. Rev. B **98**, 224423 (2018).

[5] S. Ghara, B.-G. Jeon, K. Yoo, K. H. Kim, and A. Sundaresan, Reentrant spin-glass state and magnetodielectric effect in the spiral magnet $BiMnFe_2O_6$, Phys. Rev. B **90**, 024413 (2014).

[6] L. E. Wenger and P. H. Keesom, Calorimetric investigation of a spin-glass alloy: CuMn, Phys. Rev. B **13**, 4053 (1976).

[7] R. Kumar, P. Yanda, and A. Sundaresan, Cluster-glass behavior in the two-dimensional triangular lattice Ising-spin compound $Li_2Mn_3O_7$, Phys. Rev. B **103**, 214427 (2021).

[8] Z. Ma, J. Wang, Z. Y. Dong, J. Zhang, S. Li, S. H. Zheng, Y. Yu, W. Wang, L. Che, K. Ran, S. Bao, Z. Cai, P. Čermák, A. Schneidewind, S. Yano, J. S. Gardner, X. Lu, S. L. Yu, J. M. Liu, S. Li, J. X. Li, and J. Wen, Spin-Glass Ground State in

a Triangular-Lattice Compound $YbZnGaO_4$, Phys. Rev. Lett. **120**, 087201 (2018).

[9] S. Chillal, Y. Iqbal, H. O. Jeschke, J. A. Rodriguez-Rivera, R. Bewley, P. Manuel, D. Khalyavin, P. Steffens, R. Thomale, A. T. M. N. Islam, J. Reuther, and B. Lake, Evidence for a three-dimensional quantum spin liquid in $PbCuTe_2O_6$, Nat. Commun. **11**, 2348 (2020).

[10] I. S. Hagemann, Q. Huang, X. P. A. Gao, A. P. Ramirez, and R. J. Cava, Geometric Magnetic Frustration in $Ba_2Sn_2Ga_3ZnCr_7O_{22}$: A 2d Spinel Based Kagome Lattice, Phys. Rev. Lett. **86**, 894 (2001).

[11] Y. Okamoto, M. Nohara, H. Aruga-Katori, and H. Takagi, Spin-Liquid State in the $S = 1/2$ Hyperkagome Antiferromagnet $Na_4Ir_3O_8$, Phys. Rev. Lett. **99**, 137207 (2007).

[12] N. Lakshminarasimhan, A. K. N. Kumar, S. S. Chandrasekaran, and P. Murugan, Structure-magnetic property relations in $FeNbO_4$ polymorphs: A spin glass perspective, Prog. Solid State Chem. **54**, 20 (2019).

[13] C. Meneghini, S. Ray, F. Liscio, F. Bardelli, S. Mobilio, and D. D. Sarma, Nature of "Disorder" in the Ordered Double Perovskite Sr_2FeMoO_6, Phys. Rev. Lett. **103**, 046403 (2009).

[14] J. Kroder, K. Manna, D. Kriegner, A. S. Sukhanov, E. Liu, H. Borrmann, A. Hoser, J. Gooth, W. Schnelle, D. S. Inosov, G. H. Fecher, and C. Felser, Spin glass behavior in the disordered half-Heusler compound IrMnGa, Phys. Rev. B **99**, 174410 (2019).

[15] P. Bag, P. R. Baral, and R. Nath, Cluster spin-glass behavior and memory effect in $Cr_{0.5}Fe_{0.5}Ga$, Phys. Rev. B **98**, 144436 (2018).

[16] J. Choisnet, M. Hervieu, B. Raveau, and P. Tarte, Two polymorphous lithium stannoferrites $LiFeSnO_4$: A ramsdellite-type and a hexagonal close-packed structure, J. Solid State Chem. **40**, 344 (1981).

[17] M. Greenblatt, E. Wang, H. Eckert, N. Kimura, R. H. Herber, and J. V. Waszczak1, Lithium insertion compounds of the high- and low-temperature polymorphs of $LiFeSn0_4$, Inorg. Chem. **24**, 1661 (1985).

[18] N. Jayaprakash, N. Kalaiselvi, and Y. K. Sun, Combustion synthesized $LiMnSnO_4$ cathode for lithium batteries, Electrochem. Commun. **10**, 455 (2008).

[19] M. V. V. M. Satya Kishore, U. V. Varadaraju, and B. Raveau, Electrochemical performance of $LiMSnO_4$ (M = Fe, In) phases with ramsdellite structure as anodes for lithium batteries, J. Solid State Chem. **177**, 3981 (2004).

[20] P. Lacorre, M. Hervieu, J. Pannetier, J. Choisnet, and B. Raveau, Neutron diffraction study of $Li_{1+x}(Li_{2x3}Fe_{1-x}Sn_{1+x3})O_4$, a nonstoichiometric ramsdellite and its transition to a double hexagonal close packed structure for $x = 0$, J. Solid State Chem. **50**, 196 (1983).

[21] J. R. Carvajal, FULLPROF: A program for rietveld refinement and pattern matching analysis, in *Abstract of the Satellite Meeting on Powder Diffraction of the XV Congress of the IUCr, Toulouse, France* (1990), p. 127.

[22] J. Choisnet, M. Hervieu, B. Raveau, and P. Tarte, Structural relationships in close-packed AB_2O_4 oxides involving spinel, olivine, and hexagonal $LiFeSnO_4$ structures, J. Solid State Chem. **45**, 280 (1982).

[23] M. Bandyopadhyay and S. Dattagupta, Memory in nanomagnetic systems: Superparamagnetism versus spin-glass behavior, Phys. Rev. B **74**, 214410 (2006).

[24] J. R. L. De Almeida and D. J. Thouless, Stability of the Sherrington-Kirkpatrick solution of a spin glass model, J. Phys. A. Math. Gen. **11**, 983 (1978).

[25] M. A. V. Heringer, D. L. Mariano, D. C. Freitas, E. Baggio-Saitovitch, M. A. Continentino, and D. R. Sanchez, Spin-glass behavior in $Co_3Mn_3(O_2BO_3)_2$ ludwigite with weak disorder, Phys. Rev. Mater. **4**, 064412 (2020).

[26] S. Kitani, M. Tachibana, and H. Kawaji, Spin-glass-like behavior in ferromagnetic phase of $CdCr_2S_4$, Solid State Commun. **179**, 16 (2014).

[27] S. Chowki, S. Rayaprol, A. Mukhopadhyay, and N. Mohapatra, Coexistence of spin glass type freezing and cooperative paramagnetic state in Sr_3MnTiO_7, Phys. Rev. B **92**, 214416 (2015).

[28] R. Wiebe, E. Greedan, P. Kyriakou, M. Luke, S. Gardner, A. Fukaya, M. Gat-Malureanu, L. Russo, T. Savici, and J. Uemura, Frustration-driven spin freezing in the $S = 1/2$ Fcc perovskite Sr_2MgReO_6, Phys. Rev. B **68**, 134410 (2003).

[29] U. Tutsch, O. Tsyplyatyev, M. Kuhnt, L. Postulka, B. Wolf, P. T. Cong, F. Ritter, C. Krellner, W. Aßmus, B. Schmidt, P. Thalmeier, P. Kopietz, and M. Lang, Specific Heat Study of 1d and 2d Excitations in the Layered Frustrated Quantum Antiferromagnets $Cs_2CuCl_{4-X}Br_x$, Phys. Rev. Lett. **123**, 147202 (2019).

[30] J. C. Lasjaunias, A. Sulpice, K. Biljaković, D. Vengust, and D. Mihailovič, Low-Energy vibrational excitations of $Mo_6S_3I_6$ nanowires revealed by low-temperature specific heat, Nanotechnology **18**, 355704 (2007).

[31] Y. Singh, Y. Tokiwa, J. Dong, and P. Gegenwart, Spin liquid close to a quantum critical point in $Na_4Ir_3O_8$, Phys. Rev. B **88**, 220413(R) (2013).

[32] C. Bansal and V. Srinivasan, Low energy excitation in spin glasses, Solid State Commun. **49**, 455 (1984).

[33] B. Maji, K. G. Suresh, and A. K. Nigam, Low temperature cluster glass behavior in Nd_5Ge_3, J. Phys. Condens. Matter **23**, 506002 (2011).

[34] D. Li, Y. Shiokawa, Y. Homma, A. Uesawa, A. Dönni, T. Suzuki, Y. Haga, E. Yamamoto, T. Honma, and Y. Ōnuki, Evidence for the formation of the spin-glass state in U_2PdSi_3, Phys. Rev. B **57**, 7434 (1998).

[35] A. Malinowski, V. L. Bezusyy, R. Minikayev, P. Dziawa, Y. Syryanyy, and M. Sawicki, Spin-Glass Behavior in Ni-Doped $La_{1.85}Sr_{0.15}CuO_4$, Phys. Rev. B **84**, 024409 (2011).

[36] A. P. Ramirez, Strongly geometrically frustrated magnets, Annu. Rev. Mater. Sci. **24**, 453 (1994).

[37] A. P. Young and H. G. Katzgraber, Absence of an Almeida-Thouless Line in Three-Dimensional Spin Glasses, Phys. Rev. Lett. **93**, 207203 (2004).

[38] M. Sasaki, P. E. Jönsson, H. Takayama, and H. Mamiya, Aging and memory effects in superparamagnets and superspin glasses, Phys. Rev. B **71**, 104405 (2005).

[39] S. Chakraverty, M. Bandyopadhyay, S. Chatterjee, S. Dattagupta, A. Frydman, S. Sengupta, and P. A. Sreeram, Memory in a magnetic nanoparticle system: Polydispersity and interaction effects, Phys. Rev. B **71**, 054401 (2005).

[40] Y. Sun, M. B. Salamon, K. Garnier, and R. S. Averback, Memory Effects in an Interacting Magnetic Nanoparticle System, Phys. Rev. Lett. **91**, 167206 (2003).

[41] S. Pal, K. Kumar, A. Banerjee, S. B. Roy, and A. K. Nigam, Field-cooled state of the canonical spin glass revisited, Phys. Rev. B **101**, 180402(R) (2020).

[42] J. A. Mydosh, Spin glasses: Redux: An updated experimental/materials survey, Reports Prog. Phys. **78**, 052501 (2015).

[43] V. K. Anand, D. T. Adroja, and A. D. Hillier, Ferromagnetic cluster spin-glass behavior in $PrRhSn_3$, Phys. Rev. B **85**, 014418 (2012).

[44] J. Lago, S. J. Blundell, A. Eguia, M. Jansen, and T. Rojo, Three-dimensional heisenberg spin-glass behavior in $SrFe_{0.90}C_{o0.10}O_{3.0}$, Phys. Rev. B **86**, 064412 (2012).

[45] N. Marcano, P. A. Algarabel, L. Fernández Barquín, J. P. Araujo, A. M. Pereira, J. H. Belo, C. Magén, L. Morellón, and M. R. Ibarra, Cluster-glass dynamics of the Griffiths phase in $Tb_{5-x}La_xSi_2Ge_2$, Phys. Rev. B **99**, 054419 (2019).

[46] J. Souletie and J. L. Tholence, Critical slowing down in spin glasses and other glasses: Fulcher versus power law, Phys. Rev. B **32**, 516 (1985).

[47] S. Shtrikman and E. P. Wohlfarth, The theory of the Vogel-Fulcher law of spin glasses, Phys. Lett. A **85**, 467 (1981).

[48] J. L. Tholence, Recent experiments about the spin-glass transition., Phys. B **126 B-C**, 157 (1984).

[49] P. Beauvillain, C. Chappert, and J. P. Renard, Critical behavior in an insulating spin glass: Field expansion and scaling,, J. Phys. Lettres **45**, 665 (1984).

[50] J. Nogués and I. K. Schuller, Exchange Bias, J. Magn. Magn. Mater. **192**, 203 (1999).

[51] J. Sort, J. Nogues, S. Surinach, J. S. Munoz, and M. D. Baro, Coercivity and squareness enhancement in ball-milled hard magnetic-antiferromagnetic composites, Appl. Phys. Lett. **79**, 1142 (2001).

[52] V. Kuncser, M. Valeanu, G. Schinteie, G. Filoti, I. Mustata, C. P. Lungu, A. Anghel, H. Chiriac, R. Vladoiu, and J. Bartolome, Exchange bias and spin valve systems with Fe–Mn antiferromagnetic pinning layers, obtained by the thermo-ionic vacuum arc method, J. Magn. Magn. Mater. **320**, 226 (2008).

[53] J. Sort, S. Suriñach, J. S. Muñoz, M. D. Baró, J. Nogués, G. Chouteau, V. Skumryev, and G. C. Hadjipanayis, Improving the energy product of hard magnetic materials, Phys. Rev. B **65**, 174420 (2002).

[54] M. Ali, P. Adie, C. H. Marrows, D. Greig, B. J. Hickey, and R. L. Stamps, Exchange bias using a spin glass, Nat. Mater. **6**, 70 (2007).

[55] S. Karmakar, S. Taran, E. Bose, B. K. Chaudhuri, C. P. Sun, C. L. Huang, and H. D. Yang, Evidence of intrinsic exchange bias and its origin in spin-glass-like disordered $L_{0.5}Sr_{0.5}MnO_3$ manganites (L = Y, $Y_{0.5}Sm_{0.5}$, and $Y_{0.5}La_{0.5}$), Phys. Rev. B **77**, 144409 (2008).